Temporal Differentiation of Extracellular Vesicles by Metabolic Glycan Labeling-Assisted Microfluidics

Qiuyue Wu[1], Wencheng Wang[1], Chi Zhang[1], Zhenlong You[1], Yinyan Zeng[1], Yinzhu Lu[1], Suhui Zhang[1], Xingrui Li[1], Chaoyong Yang[1,2], and Yanling Song[1]*

[1]State Key Laboratory of Physical Chemistry of Solid Surfaces, Key Laboratory for Chemical Biology of Fujian Province, The MOE Key Laboratory of Spectrochemical Analysis & Instrumentation, Department of Chemical Biology, College of Chemistry and Chemical Engineering, Xiamen University, Xiamen 361005, P. R. China.

[2] Institute of Molecular Medicine, Renji Hospital, Shanghai Jiao Tong University School of Medicine, Shanghai, 200127, China
*e-mail: ylsong@xmu.edu.cn

Extracellular vesicle (EV)/exosome secretion is a dynamic process that tunes the cellular communication for response to internal and external cues. The selective enrichment of a newly synthesized EV/exosome has been hindered by the basic fact that all EVs/exosomes, new and old, share the similar inherent parameters and thus are indistinguishable. Here, we developed a method by cotranslational introduction of azide groups into EV/exosome proteins as a timestamp and label them with biotin tag by click chemistry, to separate the newly synthesized EVs/exosomes from preexisting populations by streptavidin-modified herringbone microfluidic chip. For mouse model of anti-PD-L1 immunotherapy, the level of newly synthesized PD-L1^{+} EVs detected by the developed approach was superior to the total PD-L1^{+} EVs from mixed time sources (quantified by classical method) for tumor progression. This method makes it possible to address the temporal characteristics of newly synthesized EVs/exosomes in cell and *in vivo*, for studying EV/exosome secretion to respond to specific stimuli.

All cells secrete extracellular vesicles (EVs) as part of their normal physiology and during acquired abnormalities[1]. Exosomes are nanoscale (~40 to 160 nm in diameter) EVs which are crucial to regulate intercellular communication[2]. Precise exosome transmission underlies fundamental physiological processes, which rely on the parent cell and recipient cell to maintain homeostasis or to adapt to received stimuli [1, 3, 4]. Abnormal exosome secretion has been found in many diseases, such as cancer progression, cardiovascular diseases, neuro-degenerative diseases and viral pathogenicity [2, 5, 6]. The essence of this phenomenon is largely focused on the regulation of exosome production for response to internal and external cues. The exosome secretion and uptake are dynamic, resulting in net production of a mixed exosome population consisting of both newly synthesized exosomes to response specific stimuli and “outdated” exosomes synthesized before the stimuli. Studies of exosome dynamics would be facilitated by strategies that enable selectively quantitation of newly synthesized exosomes from preexisting exosome pool, that permits a survey of the primary exosome synthesis response to specific stimulus. These findings not only contribute to substantially improve our understanding of the biology role of exosome in cell-to-cell communication, but also inform the potential exosome biomarkers for disease progression and response to therapy.

Quantifying newly generated exosomes response to a stimulus is challenged by the dynamic process of the de novo production and by the large amount population of "old" exosomes. Classical methods for exosome separation rely on exosome physical properties (for example, sedimentation rate-based ultracentrifugation and size-based microfiltration) or exosomal specific proteins (for example, affinity-based magnetic bead/microfluidic enrichment) [7-13]. The separation relies a set of exosome inherent parameters that are independent to temporal resolution, which is unable to selectively enrich exosomes of different temporal origins. Time-lapse monitoring of exosome concentration from cultured cells provides a means of study exosome dynamics, but eliminating the exosome exchange under physiological conditions which is critical for understanding *in vivo* exosome-mediated intercellular communication. As a result, it is remains poorly understood whether newly synthesized exosomes have production rate and molecular alterations compared to old exosomes, resulting in distinct localization, recipient cell's metabolic status, and/or exosomal function outcomes. Therefore, some findings will be refined as new quantification technology for newly synthesized exosome is embraced.

Here, we developed a method based on metabolic labeling assisted timestamp and click chemistry mediated microfluidic separation (CATCH) to allow selectively enrich newly synthesized exosomes response to immunotherapy (Scheme 1). *In vivo* metabolic glycoengineering with unnatural sugars is performed at the same time as specific stimuli (e.g. anti-PD-L1 immunotherapy), affording the opportunity to differentiate newly synthesized exosomes from preexisting exosome populations by ubiquitously tagging them with bioorthogonal functional groups (similar to setting timestamps to letters). Through subsequent click chemistry between exosomal chemical functional groups (azide) and alkynyl biotin, newly synthesized exosomes are labeled with biotin allowing their separation from the preexisting exosomes by streptavidin-modified herringbone microfluidic chip. As a result, the relative amounts of exosomes that are produced after each immunotherapy administration can be quantitated by microfluidic separation and antibody staining, by sequential administration and corresponding metabolic pulse labeling.

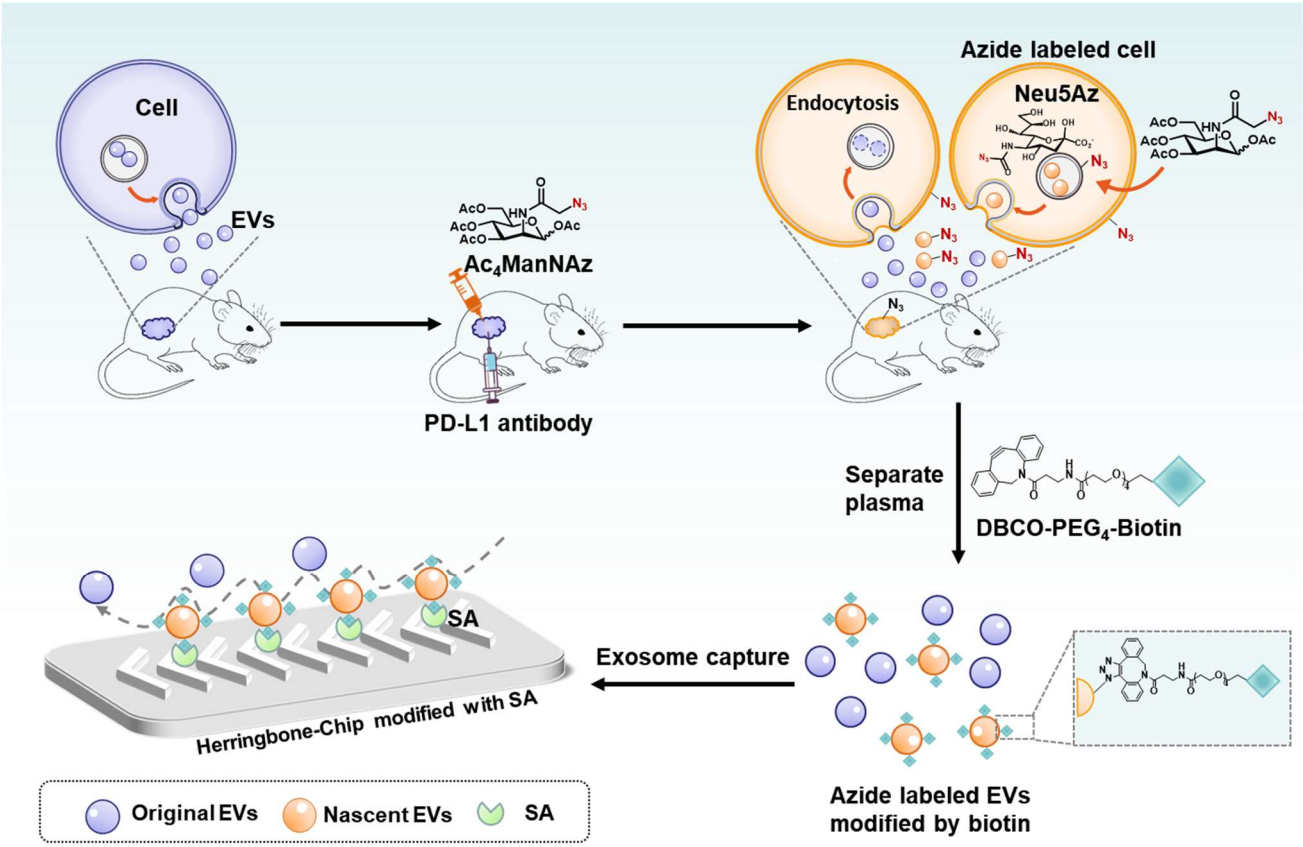

Scheme 1. Schematic illustrating the strategy to study dynamic changes of newly synthesized EVs in vivo after immunotherapy based on metabolic labeling. Mice were subcutaneously injected with 4T1 cells, and then every week treated with PD-L1 antibody once or injected with PBS as a control, simultaneously injection $Ac_4ManNAz$ for unnatural glucose metabolism labeling for three consecutive days. At this time, the azide-labeled EVs in the mice were newly synthesized. After reacting with DBCO-PEG_4-Biotin linker, the newly synthesized EVs with biotin labeled can be captured by streptavidin (SA)-modified chips.

Results

Metabolic Glycan Labeling (MGL) of Exosomes *in Vitro*. An ideal timestamp should be biorthogonal, while at the same time, being biocompatible with exosomal function execution [14]. We chose $Ac_4ManNAz$ as MGL additives, an unnatural azido-containing monosaccharide that has been exploited to tag glycoproteins in cells and *in vivo* for its high labeling efficiency and good biocompatibility [15-18]. In this work, we applied $Ac_4ManNAz$ labeling as the "timestamp", which can distinguish newly synthesized from pre-existing exosomes and allow selectively covalent react to alkyne-functioned reagent through click chemistry.

To determine whether azido groups is incorporated into exosomes, we separated exosomes from $Ac_4ManNAz$-treated A375 cells by ultracentrifugation and reacted with the alkyl dye (DBCO-Cy5) (**Fig. 1a**). Subsequent flow cytometry analysis and confocal images showed the fluorescence of metabolically labelled exosomes

were obviously higher than those of standard exosomes (**Fig. 1b**), revealing the successful incorporation of azido into exosomal surface. To further assess the suitability of Ac_4ManNAz for labeling exosomes, we examined the influence of its treatment on the exosomal physical properties and protein composition. Similar to standard exosomes, the metabolically labelled exosomes had cup-shaped structures (**Fig. 1c**) with an average diameter of 140 nm and zeta potential about -4.5 mV (**Fig. 1d-e**). And metabolically labelled exosomes have a high expression level of CD63, a classical exosomal marker (**Fig. 1f**). Moreover, a total of 806 mutual proteins of 1000 total proteins were found between exosomes with/without MGL (**Fig. 1g**). Gene ontology analysis of proteins and annotated their biological process (**Fig. 1h**), cellular component (**Fig. 1i**) and molecular function (**Fig. 1j**), indicating the protein of exosomes with/without MGL are expressed very similarly. In addition, we demonstrate that MGL for exosome is highly reproducible between biological replicates (correlation, 0.99, **Fig. 1k-l**), allowing for statistical evaluation. Overall, Ac_4ManNAz exposure seems to be biologically compatible for exosome, and does not appreciably affect exosomal morphology and proteome.

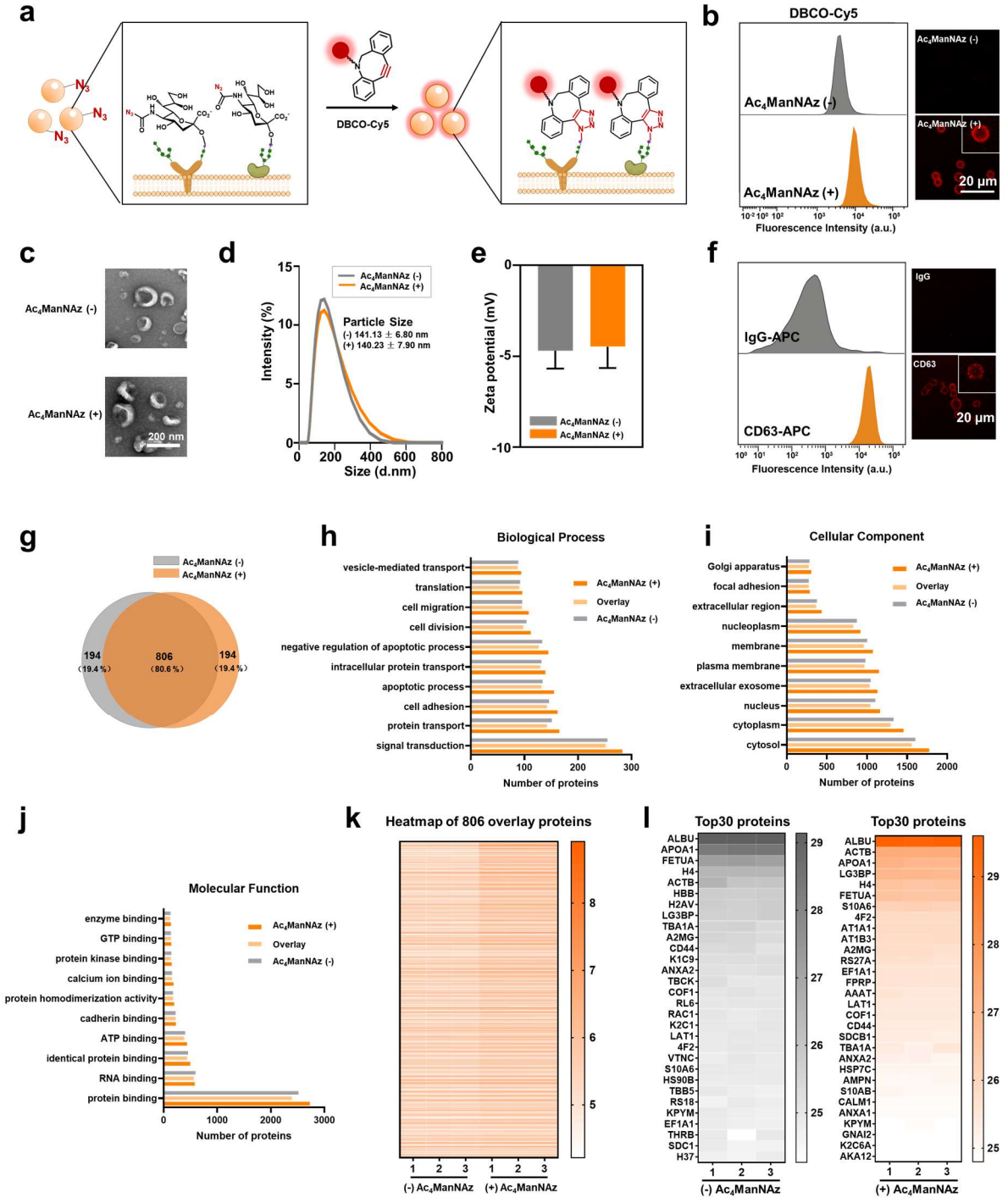

Fig. 1| Identification and characterization of azide labeled or unlabeled A375 exosomes. a, Schematic diagram of azide labeled or unlabeled A375 exosomes incubated with DBCO-Cy5. **b,** Fluorescence intensity of A375 exosomes treatment with or without Ac_4ManNAz additives, and then incubated with DBCO-Cy5. **c,** Physical morphologies of azido labeled or unlabeled A375 exosomes by transmission electron microscopy (TEM), scale bar = 200 nm. **d,** Size distribution of A375 exosomes treatment with or without Ac_4ManNAz additives by Dynamic Light Scattering Instrument (DLS). **e,** Zeta potential of azido labeled or unlabeled A375 exosomes. **f,** Flow cytometry analysis and representative confocal images of the binding performances of CD63 antibody. **g,** Veen diagram displayed the overlap proteins in top 1000 proteins of A375 exosomes treated with or without Ac_4ManNAz additives. **h-j,** Biological Process (**h**), Cellular Component (**i**) and Molecular Function (**j**) of gene ontology (GO) enrichment analysis of proteins detected in A375 exosomes treated with (orange) or without (gray) Ac_4ManNAz additives, and in mutual proteins (light orange). **k,** Heatmap displaying the expression level of overlapped 806 proteins detected both azide labeled or unlabeled A375 exosomes. The log10 expression values for the overlapped proteins are indicated by colors as shown in the scale. **l,** Heat map of top 30 proteins within 3 biological replicates of A375 exosomes treated with (orange) or without (gray) Ac_4ManNAz additives. The log2 expression value for the top 30 proteins are indicated by colors as shown in the scale.

Microfluidic Isolation of Metabolically Labelled Exosomes. To test the ability of metabolically labelled exosomes to be captured, the alkyl biotin (DBCO-PEG_4-biotin) was applied to bio-orthogonally react with the exosomal azide groups introduced by MGL. Biotin lagged exosomes were then enrichened by streptavidin (SA) modified herringbone microchip (HB-Chip)[10 19 20], a high-throughput microfluidic mixing device to promote mass transfer of biotin tagged newly synthesized exosomes to the streptavidin functioned surface (**Fig. 2a**). As shown in the simulation (**Fig. 2b**), the designed chip with herringbone patterned channels could disrupt the laminar flow profile and generate steady chaotic flows, which enhances the collision between exosomes and affinity interface.

As a result, labeling exosomes with azido by MGL, allow covalent reaction of alkyne-biotin reagent and selective capture by SA functioned HB-Chip. While pre-existing exosomes before MGL can be washed away due to the lack of biotin. The fluorescence intensity was obtained by sequentially introduction of anti-CD63, β-galactosidase conjugated secondary antibody and FDG (**Fig. 2a**). By metabolic labeling assisted timestamp and click chemistry mediated separation (CATCH), the fluorescence intensity of exosomes from MGL treated cells was ~3.5 times higher than that of exosomes without MGL (**Fig. 2c, d**). Moreover, a response curve for different concentrations of exosomes from Ac_4ManNAz-treated cells with a good linear relation (R^2=0.96, LOD=12.50 ng/μL), suggesting that the CATCH strategy can quantitatively detect metabolically labelled exosomes (**Fig. 2e**). And the exosomes captured by CATCH maintain a spherical topology (**Fig. 2f**). In addition, 3D fluorescence images-based reconstructions indicated that pre-stained exosomes with MGL could be captured by the HB-Chip, while exosomes without metabolic labeling were not (**Fig. 2g**), again highlighting the good selectivity of CATCH strategy.

The time window of the CATCH strategy was then explored. The exosomes collected under different time of MGL-treated cells (ranging from 0-36 h) were analyzed by CATCH, which showed that the obtained signal intensity increased with time (**Fig. 2h**). After the addition of Ac_4ManNAz for 4 hours, the collected exosomes from A375 cells could be captured by the CATCH method and showed obvious signals compared with the untreated exosomes ($P < 0.001$). The four-hour time window ensures the basic consistency of metabolic glycan labeling and the timing of specific stimuli.

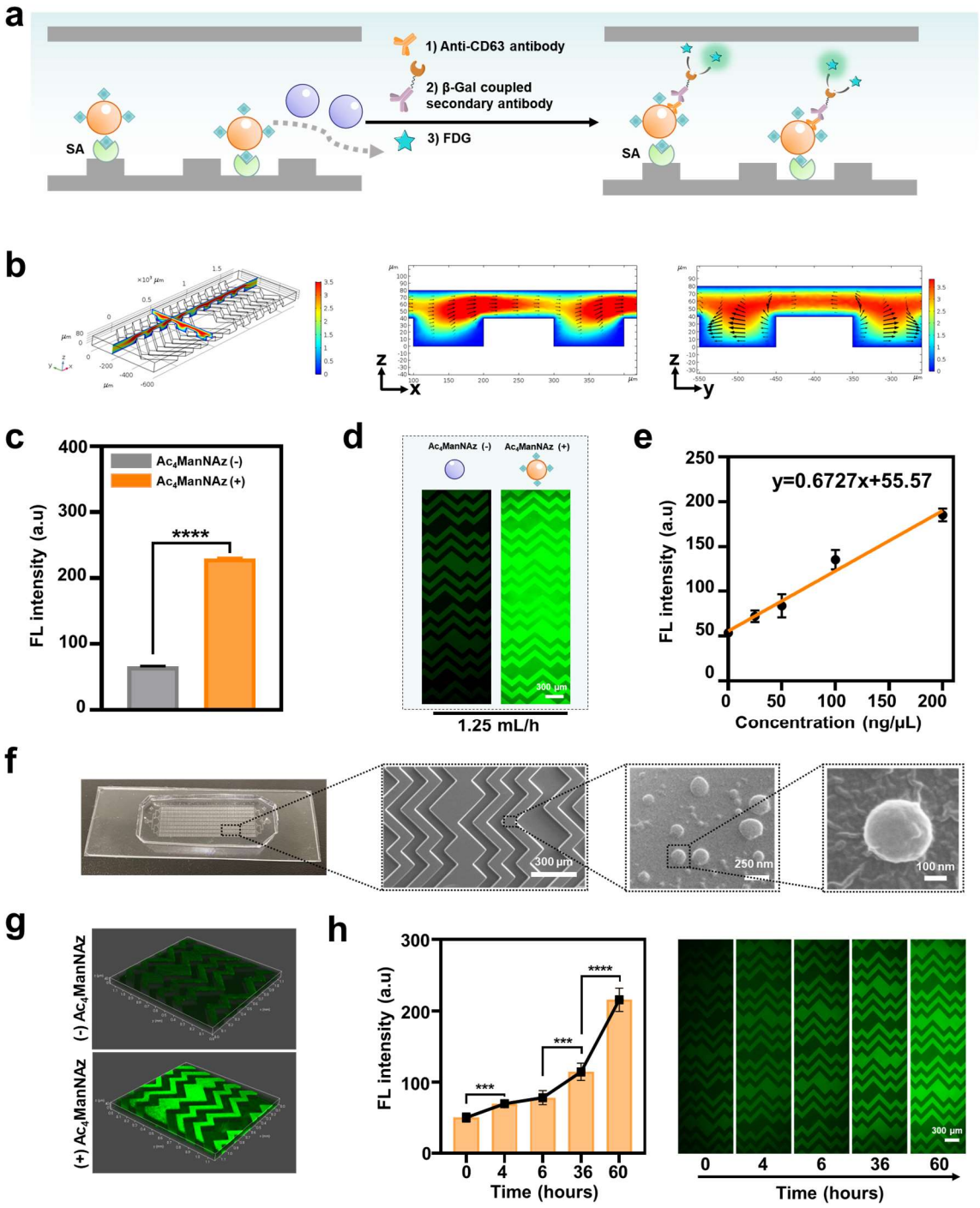

Fig. 2| Capture performance and working curves of A375 exosomes on the chip. a, The diagram illustrates that exosomes modified with azide can be captured by SA modified chip after reaction with DBCO-PEG$_4$-Biotin. The captured exosomes bind to the anti-mouse CD63 primary antibody, and then bind to the secondary antibody labeled with β-galactosidase (β-Gal). Following by adding substrate FDG, fluorescence signals can be collected by Nikon Fluorescence microscope. Then the expression level of CD63 protein was detected. **b,** Numerical simulation of velocity streamline and turbulence flow formed on microgrooves in Z–X and Z–Y vertical cross-section of the herringbone chip channels. **c,** Optimal flow rate for azide labeled exosome capture by chip. **** $P < 0.0001$ **d,** Fluorescence microscopy of the effect of antibody binding of exosomes captured by chip at 1.25 mL/h. **e,** The operating curve of captured exosomes on the chip. **f,** Picture of fishbone chip, and its surface morphology and captured exosomes were displayed by Scanning Electron Microscope (SEM). **g,** 3D confocal fluorescence microscopy showing the DiI-stained exosomes captured inside herringbone chips. **h,** The time curve of captured exosomes on the chip and representative fluorescence images at different time points (0 h, 4 h, 6 h, 36 h, 60 h). ***$P < 0.001$, **** $P < 0.0001$

Isolation of Metabolically Labelled Exosomes/Extracellular Vesicles from Mouse Plasma.

To demonstrate that metabolically labelled exosomes or extracellular vesicles in mice can be isolated by CATCH strategy, a mouse 4T1 breast cancer model was constructed. *In vivo* metabolic labeling was performed for three consecutive days from the 24th day, and then mouse plasma and tumor tissue were collected on day 27 respectively (**Fig. 3a**). Tumor tissue-derived extracellular vesicles (EVs) were separated from the tissue structure by using a combination of enzymes and tissue slicing, and then isolated by differential ultracentrifugation (**Fig. 3b**). Then, five μL mouse plasma or five μg tumor tissue-derived EVs were bioorthogonally react with DBCO-PEG$_4$-biotin, and injected into the SA functioned HB-Chips for analysis. Similar to the results of *in vitro* metabolic labeling, the unlabeled mouse samples had significantly lower anti-CD63 stanning intensity than those in the corresponding metabolically labeled samples in both plasma and tissue (**Supplementary Fig. 1, Fig. 3c**). Considering that the signal intensities of plasma were quite close the tumor tissue-derived EVs of the same mouse, and that plasma does not require a complicated pre-isolation process, mouse plasma was used as the sample in subsequent experiments. Together, these results suggest that CATCH strategy could not only capture cell-derived exosomes, but also directed isolate metabolically labelled EVs from mouse plasma.

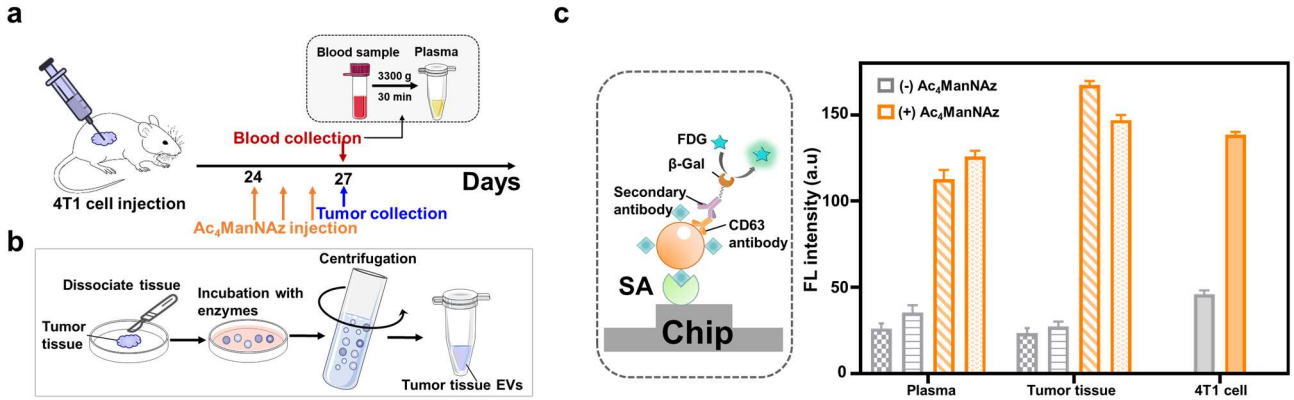

Fig. 3| Validation of metabolically labeled effect of 4T1 EVs *in vitro* and *in vivo*. a, Schematic schedule of tumor implantation mice in vivo experiments. **b,** The protocol of EVs collected from tumor tissue. **c,** Fluorescence intensity of newly synthesized EVs from plasma, tumor tissue and 4T1 cell captured by SA-modified chip. The same pattern on each column represents the sample collected from the same mouse.

Dynamic Changes of Newly Synthesized EVs in Response to PD-L1 Immunotherapy.

Tumour cells evade immune surveillance by upregulating the programmed death-ligand 1 (PD-L1) expression [21]. PD-L1 antibody-based immunotherapy has shown remarkable promise in tumor treatments [22]. Nevertheless, the favorable response rate in clinical is low [23]. One important reason is that exosomal PD-L1 has been found as a major regulator of tumor progression through suppressing T cell activity and appears to be

resistant to PD-L1 immunoblockade [24-26]. Understanding how responds the PD-L1 exosomes/EVs to PD-L1 antibody immunotherapy will be an important avenue of research going forward. For this purpose, we applied CATCH strategy to isolate of newly synthesized EVs from a large amount of the "outdated" EVs, revealing the temporal EV response to PD-L1 immunotherapy.

Mouse 4T1 breast tumor model, a suitable animal model for human primary/metastatic breast cancer, was chosen for PD-L1 immunotherapy. First, we confirmed the expression of PD-L1 in 4T1 cell (**Supplementary Fig. 2**) and demonstrated the feasibility of using CATCH strategy to selectively capture metabolically labelled PD-L1$^+$ EVs from 4T1 murine plasma (**Supplementary Fig. 3**). Second, 4T1 tumor mouse was treated with PD-L1 antibody or PBS as a negative control on day 7, and every 7 day thereafter (**Fig. 4a**). Meanwhile, Ac_4ManNAz were simultaneously injected with immunotherapy for three consecutive days to refine a "chemical timestamp" to differentiate newly synthesized EVs from the large amount of the "outdated" EVs after PD-L1 immunotherapy. During this process, tumor growth trends were suppressed in the anti-PD-L1-treated group compared to that of the untreated group (**Fig. 4b, Supplementary Fig. 4**). The results of hematoxylin-eosin (HE) and immunofluorescence staining further demonstrated the effective anti-PD-L1 immunotherapy (**Fig. 4c**), specifically with increased apoptotic cells (anti-TUNEL staining) and infiltration of CD8$^+$ T cells (anti-CD8 staining), accompanied by decreased cancer cells (anti-Ki67 staining).

Then, the collected plasma with/without anti-PD-L1 treatment were analyzed by CATCH strategy. There was no significant difference in the number of new total EVs quantified by CD63 antibody between the treated and untreated groups, suggesting that net production of total plasma EV remains stable even with tumor growth and drug stimulation (**Fig. 4d**). Interestingly, when the detection antibody was replaced by anti-PD-L1, treatment or not had a significant difference in the amount and production rate of newly synthesized PD-1 EVs, even though they tended to be stable in the first two weeks and increased in the third week (**Fig. 4e)**. Nevertheless, different from the trend of new PD-L1 EVs, the total PD-L1 EVs (captured by CD63 antibody) in the un-treatment group continued to increase with time, while the treatment group only increased in the first week and maintained steady production from the second week (**Fig. 4f**). Together, the different trends of total (including old and new) and new EVs indicates that the background of large numbers of old EVs may cover the slight changes in EV secretion after immunotherapy. Importantly, compared to the total PD-L1$^+$ EVs, the level of newly synthesized PD-L1$^+$ EVs stronger positively correlated with tumor size no matter in untreated/treated group (**Fig. 4g**), which were shown to be indicative of tumor progression and therapy response. Overall, the

developed CATCH strategy improved the precision of the *in vivo* EV response to stimulation, enabling a timely and accurate reflection of the successful anti-PD-1 therapy.

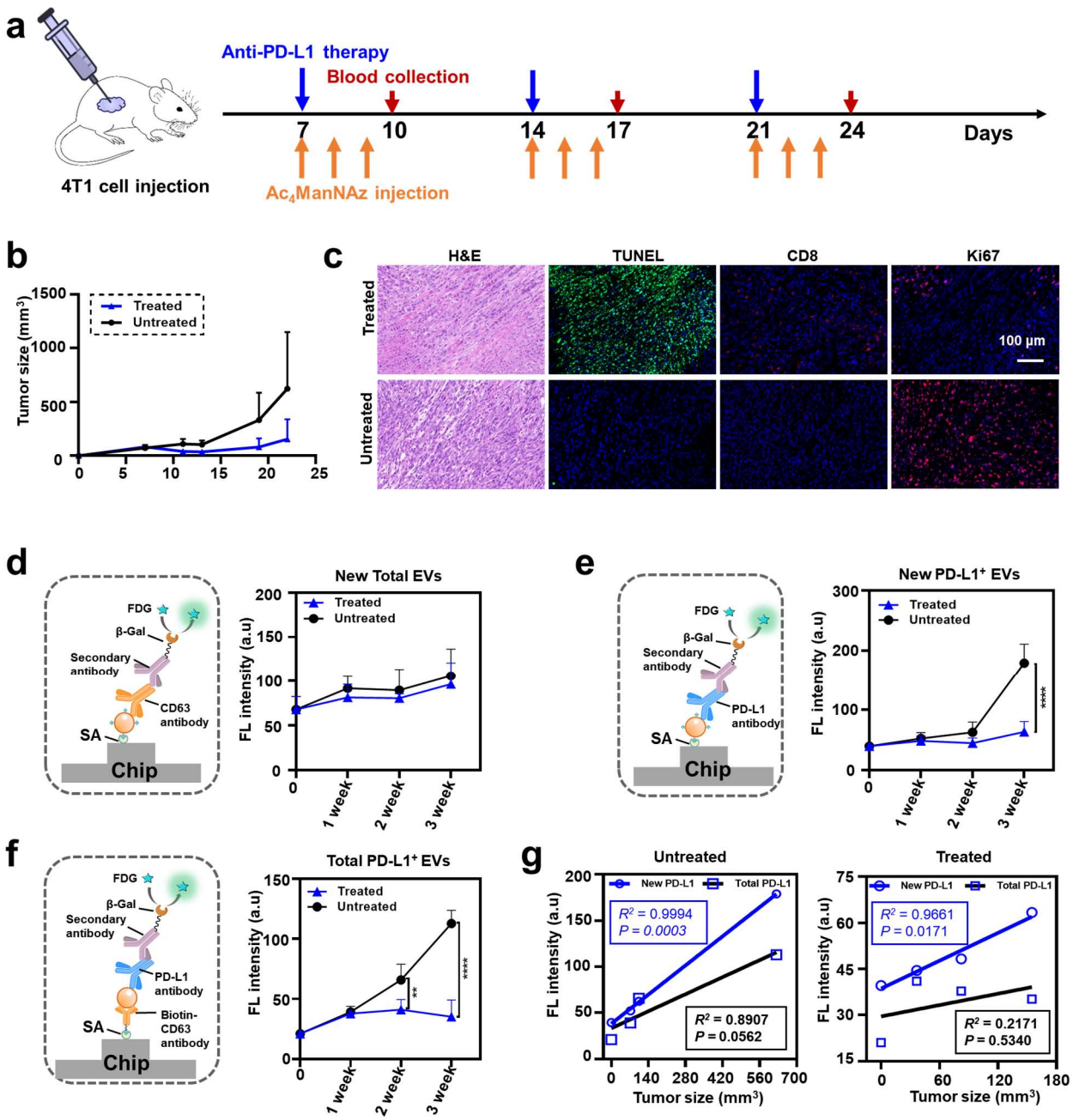

Fig. 4| The effect of immunotherapy on newly synthesized EVs in tumor mice was analyzed based on metabolic labeling strategy. a, Schematic schedule of mice in vivo experiments. Blue arrows indicate time points of anti-PD-L1 therapy. Orange arrows indicate time points of $Ac_4ManNAz$ injection. Red arrows indicate time points of blood collection. **b,** Tumor growing curve of the mice in different treatment group. **c,** Representative images revealing the immunotherapy effect on mouse tumor tissues. HE staining is a common method to differentiate between the nuclear and cytoplasmic parts of a cell, and show the general layout and distribution of cells and provides a general overview of a tissue sample structure thus providing more histologic information. TUNEL assay is a method for detecting apoptotic DNA fragmentation, widely used to identify and quantify apoptotic cells in tumor tissues. $CD8^+$ T cell also known as cytotoxic T lymphocyte (CTL) is a T lymphocyte (a type of white blood cell) that kills cancer cells, cells that are infected by intracellular pathogens (such as viruses or bacteria), or cells that are damaged in other ways. The Ki-67 protein is a cellular marker for proliferation and is commonly used to estimate the tumor cell proliferation. **d,** Levels of newly synthesized total EVs at different stages of indicative treatment. **e,** Levels of newly synthesized PD-$L1^+$ EVs at different stages. **** $P < 0.0001$ **f,** Levels of total PD-$L1^+$ EVs at different stages. ** $P < 0.01$, **** $P < 0.0001$ **g,** Pearson correlation of the newly synthesized PD-$L1^+$ EVs (blue line) and total PD-$L1^+$ EVs (black line) to the tumor size in 4T1 breast cancer mice with or without PD-L1 treatment.

Discussion

A thorough understanding of EV/exosome function requires a dynamic view. Temporal resolution is essential if one is to describe the dynamic responses of EV/exosomes to specific stimulus. Elucidating these dynamic changes in the net production of EV/exosome at a given state is a challenge requiring specialized techniques, which should be biocompatible and sensitive enough to specifically quantify subtle changes in EV/exosome production. Taking a series of "snapshots" of EV/exosome productions will help us to understand the temporal dynamics, which will provide invaluable insights for treatment assessment, progression monitoring, and drug development.

Unique to the CATCH approach are the selective labeling and isolation of the newly synthesized EVs/exosomes, thereby raising the chances of accurately revealing EV/exosome changes in response to treatment. The strength of the approach lies in that metabolic glycan labelling facilitates the efficient differentiate new EVs/exosomes against a bewildering background of preexisting EVs/exosomes. Through subsequent click chemistry and mixing-accelerated herringbone chip, newly synthesized EVs/exosomes can be selectively and sensitively quantification. We demonstrate the metabolic glycan labelling of EV/exosome is biologically compatible (labeling does not appreciably affect exosomal morphology and proteome) and efficient (4 h of labeling were sufficient to identify secretory exosomes). Moreover, the proposed CATCH approach enables selectively detection of net production of newly synthesized total EVs and new PD-L1^{+} EVs after each anti-PD-L1 administration. As a result, the level of newly synthesized PD-L1^{+} EVs was identified to be a more accurate tumor progression marker than the total PD-L1^{+} EVs from mixed time sources. Overall, that the combination of EV/exosome metabolic labelling and efficient microfluidic enrichment improve the ability to analyze EV/exosome secretion over time spans, which will be helpful to study EV/exosome secretion mechanisms, as well as for in-depth exploration of the biological functions and clinical value of EVs/exosomes from different time sources.

Methods

Materials and cell lines. Human melanoma A375 cells and human glioma U251 cells were purchased from American Type Culture Collection (ATCC). Murine breast cancer 4T1 cell lines was Procell Life Science & Technology Co.,Ltd. (Wuhan, China). Sterile PBS buffer (E607008-0500), Glycine and 4% Paraformaldehyde Fix Solution(E672002-0500) were purchased from Sangon Biotech (ShangHai, China). Dulbecco's Modified Eagle Medium (DMEM) and RPMI 1640 medium were purchased from Cytiva (Shanghai, China). Fetal bovine serum (FBS) was purchased from Biological Industries (BI) (Shanghai, China), Penicillin Streptomycin Glutamine was purchased from Gibco (USA). BCA protein

assay kit was purchased from Epizyme Biomedical Technology Co., Ltd (Shanghai, China). N-azidoacetylmannosamine-tetraacylated ($Ac_4ManNAz$) was purchased from Shanmu Biological Medicine (Jinan, China). DBCO-PEG_4-Biotin and Collagenase D were purchased from Sigma-Aldrich (USA). Aldehyde/sulfate latex beads, bovine serum albumin (BSA), n-γ-maleimidobutyryl-oxysuccinimide ester (GMBS), SuperBlock™ Blocking Buffers and anti-human CD63 APC antibody were purchased from Thermo Fisher Scientific Inc. IgG-APC was purchased from Santa Cruz (Texas, USA.). Anti-mouse CD63 antibody was purchased from R&D systems (USA). FDG was purchased from AAT Bioquest (USA), Mouse anti-Human CD63 was purchased from BD Pharmingen (USA), anti-PD-L1 antibody was purchased from Novus Biologicals (USA) and goat anti-mouse IgG H&L (beta-galactosidase) and Rabbit Anti-Rat IgG H&L (beta-galactosidase) were purchased from Abcam (USA). Streptavidin (SA), 3-Mercaptopropyltri-methoxysilane (MPTS) and Dimethyl sulfoxide (DMSO) were purchased from Sigma-Aldrich (USA). 1,1'-dioctadecyl-3,3,3',3'-tetramethylindocarbocyanine perchlorate (DiI) lipophilic dye was purchased from Beyotime Biotech Inc (Shanghai, China). Phosphotungstic acid was purchased from Acmec Biochemical (Shanghai, China). EDTA K_2 Anticoagulation Tube was purchased from BD microtainer (USA). Anti-mouse PD-L1 antibody for immunotherapy was purchased from BioXCell (USA). DNase I (AC1711) was purchased from Sparkjade (Shangdong, China). DAPI (G1012) and EDTA K_2 Anticoagulation Tube (QX0001) were purchased from Servicebio (Wuhan, China).

Cell culture and exosome purification. A375 cells were cultured in DMEM supplemented with 10% (v/v) FBS and 1% Penicillin Streptomycin Glutamine. 4T1 cells were cultured in RPMI 1640 medium supplemented with 10% (v/v) FBS and 1% Penicillin Streptomycin Glutamine. For metabolic glycan labelling, the cell medium was replaced with 50 μM $Ac_4ManNAz$ contained medium after the 95% cell adhered the petri dish[14].

To obtain cell-derived exosomes, the standard cell culture medium was replaced with exosome free FBS contained medium after 95% cell adhered the petri dish. Exosomes in FBS were depleted by 18 h centrifugation at 100,000 g and supernatants was collected. For exosome acquisition at different time points, the supernatant was collected after cell proliferation for 0 h, 4 h, 6 h, 36 h, 60 h. After the supernatants were collected from cell cultures, exosomes were purified by a standard centrifugation protocol. First, cell debris and dead cells in culture supernatants were removed by centrifugation at 3,000 g for 20 min (Beckman Coulter, Allegra X-15R). Then, microvesicles were pelleted and discarded after 16,500 g centrifugation for 45 min (Beckman Coulter, Optima XE-90). Finally, the obtained supernatants were then centrifuged at 100,000 g for 2 h, the pelted exosomes were resuspended in PBS and collected by ultracentrifugation at 100,000 g for 2 h. The whole centrifugation operations were conducted at 4 ℃.

Characterization of purified exosomes. The exosome sample was dropped on a copper net and stained with phosphotungstic acid for 1 min, and then observed by transmission electron microscope (TEM) (Hitachi, ht-7700, Japan). The size distribution and zeta potential of A375 exosomes were characterized by Dynamic light scattering (DLS) (Nano-ZS). The total protein level of exosome was determined by BCA protein assay kit. To characterize the exosomal CD63 expression level, 10 μg exosomes were added into tube and mixed with 4 μL aldehyde/sulfate latex beads for 15 min at room temperature, then incubated in 1 mL PBS buffer for 60 min, and then blocked by 100 μL 1 M Glycine 20% (v/v) BSA contained PBS for about 30 min. Then they were washed twice by 0.5% (v/v) BSA contained PBS and centrifugation (6500 rpm, 5 min) (Eppendorf, Centrifuge 5424R). Finally, they were resuspended in 40 μL 0.5% (v/v) BSA contained PBS. 4 μL exosome covered beads were incubated with anti-CD63 antibody for 1 hour, while incubated with IgG as control. After washing twice with 0.5% (v/v) BSA PBS buffer, the fluorescence intensities of samples were measured by flow cytometry (BD verse) and fluorescence confocal microscopy (Leica SP8-STED 3X).

Fabrication SA modified chip. The herringbone PDMS chip was prepared according to our previous report[27, 28]. The PDMS prepolymer (m/m = 10:1) was poured into the chip mold and then baked in 135 ℃ for 5 min. After solidification, the PDMS chips were peeled from mold and punched the inlet and outlet for the following chemical modification. First, the PDMS chips were activated by oxygen plasma and successively incubated with 4% (v/v) (3-Mercaptopropyl) trimethoxysilane (MPTS) (in ethanol) for 1 hour and then washed with ethanol before dried in a 100 ℃ oven for 1 hour. Next, freshly prepared n-γ-maleimidobutyryl-oxysuccinimide ester (GMBS) was introduced into chip for 30 min. Finally, 20 μg/mL Streptavidin (SA) solution was injected into chip to produce SA-modified interface. For biotinylated anti-mouse CD63 antibody modified, the chip was incubated with 20 μg/mL antibody through the affinity between SA and biotin molecules.

Verification of metabolically glycan labelling (MGL) effect of A375 or 4T1 exosomes. To verify the MGL effect of exosomes, the Ac_4ManNAz-treated or untreated exosomes covered latex beads were incubated with 10 μM DBCO-Cy5 for 1 hour, and then detected by flow cytometry and fluorescence confocal microscopy after washing twice.

To detect if the exosomes modified with azido could be captured by SA modified herringbone PDMS chip after the reaction with DBCO-PEG_4-Biotin. 5 μg exosomes were incubated with 2.5 μM DBCO-PEG_4-Biotin in 20 μL 0.5% BSA contained PBS at 37 ℃ for 1 h. Then the samples were bumped into the chip. The uncaptured exosomes were washed away by 0.5% BSA contained PBS. To detect the capture effect, 15 μM DiI lipophilic dye in PBS buffer was used to stain the exosomes and its staining effect was confirmed by Confocal 3D Imaging (Leica SP8-STED 3X). To detect the protein expression level, the captured exosomes were incubated with the primary antibody and then bind to the secondary antibody modified with β-Gal protein, followed by adding substrate FDG, fluorescence signals can be collected by fluorescence microscope (Nikon Ti-U). Then the expression level of CD63 or PD-L1 protein was detected.

In vivo mice experiments. All animal experiments were performed according to protocols approved by Principles of Laboratory Animal Care (People's Republic of China). Feed and water were available ad libitum. Artificial light was provided in a 12 h/12 h cycle. All the BALB/c mice were purchased from Xiamen University Laboratory Animal Center. 4T1 cells were incubated with anti-mouse PD-L1 PE antibody to ensure their PD-L1 protein expression before establishing syngeneic mouse breast cancer model in BALB/c mice. 4T1 cells (2.5×10^5 cells in 100 μL sterile PBS buffer) were subcutaneously injected into immunocompetent 6-8 weeks BALB/c mice. Mice were allocated randomly to each treatment group. The dose of 12.5 mg/kg PD-L1 antibody or PBS buffer was injected intraperitoneally every 7 days[29]. 100 μL 140 mM Ac_4ManNAz was injected intraperitoneally[30] and 20 μL 25 mM was injected intratumorally[31] once daily for 3 consecutive days after antibody treatment. Mice were weighed every 3 days. Tumors were measured using a digital caliper and tumor volume was calculated by the formula[32]: $(\text{width})^2 \times \text{length} \times 0.52$. The mice were euthanized before we collected the blood samples and tumors. The tumors were kept in the 4% Paraformaldehyde Fix Solution for following HE staining. The mouse blood was kept in EDTA K_2 Anticoagulation Tube and centrifuged 1550g for 30 min to obtain cell-free plasma. The plasma samples were kept in -80 ℃ refrigerator (Thermo Scientific) before use. Tumor tissue EV were extracted according to the previous report[33]. Briefly, tumor tissue was dissociated until all pieces have a homogeneous size of approximately 2 × 2 × 2 mm, then incubated with collagenase D and DNase I at 37 ℃ for 30 min. The sterile 70 μm cell strainer on the top of a 50 mL polypropylene tube was used for filtration the mixture. Finally, the supernatant was collected by 3,000 g centrifugation (20 min, 4 ℃) to discard the cells and debris, and then tumor tissue derived EVs was collected through 100,000 g centrifugation (2 h, 4 ℃).

EV capture from mouse blood samples. For capturing the newly synthesized EVs from samples, 5 μL mouse plasma or 5 μg tumor tissue EVs were incubated 2.5 μL (100 μM) DBCO-PEG_4-Biotin in 20 μL 0.5% BSA contained PBS at 37 ℃ for 1 hour. Then the samples were bumped into chip at 1.25 mL/h. The uncaptured EVs were washed away by 0.5% BSA contained PBS. To detect the captured EVs in chip, 20 μL 20 μg/mL primary antibody was bumped into the chip and incubated for 1 h, then washed with 200 μL SuperBlock™ Blocking Buffer. 20 μL 120 μg/mL secondary antibody modified with β-Gal were injected and incubated for 1 hour, then washed with 200 μL 0.5% BSA contained PBS. Substrate FDG were added, fluorescence signals can be collected by fluorescence microscope (Nikon Ti-U). Then the expression level of CD63 or PD-L1 protein was detected.

Immunofluorescence staining. Immunofluorescence staining was performed on paraffin-embedded (FFPE) sections. For FFPE sections, antigen retrieval by steaming in citrate buffer (pH=6.0) was performed before blocking. The fixed sections were incubated with primary antibodies overnight at 4 ℃, followed by incubation with fluorophore-conjugated secondary antibodies for 1 h. The cell nuclei were stained with DAPI. Samples were observed using an Ortho-Fluorescent Microscopy (Pannoramic 250 FLASH).

Statistical analysis. All the Error bars were expressed as mean ± standard deviation. Student's t-test or one-way analyses of variance (ANOVA) were performed in statistical evaluation. Asterisks are used to indicated statistical significance (*$P < 0.05$, **$P < 0.01$, ***$P < 0.001$, ****$P < 0.0001$). n.s. is nonsignificant, $P > 0.05$.

References

1. Yáñez-Mó, M. *et al.* Biological properties of extracellular vesicles and their physiological

functions. *J Extracell Vesicles* **4**, 27066 (2015).
2. Kalluri, R. & LeBleu, V.S. The biology, function, and biomedical applications of exosomes. *Science* **367** (2020).
3. van Niel, G., D'Angelo, G. & Raposo, G. Shedding light on the cell biology of extracellular vesicles. *Nat Rev Mol Cell Biol* **19**, 213-228 (2018).
4. S, E.L.A., Mäger, I., Breakefield, X.O. & Wood, M.J. Extracellular vesicles: biology and emerging therapeutic opportunities. *Nat Rev Drug Discov* **12**, 347-357 (2013).
5. Hoshino, A. *et al.* Extracellular Vesicle and Particle Biomarkers Define Multiple Human Cancers. *Cell* **182**, 1044-1061.e1018 (2020).
6. Poudineh, M., Sargent, E.H., Pantel, K. & Kelley, S.O. Profiling circulating tumour cells and other biomarkers of invasive cancers. *Nature Biomedical Engineering* **2**, 72-84 (2018).
7. Zhao, H. *et al.* A hydrogel-based mechanical metamaterial for the interferometric profiling of extracellular vesicles in patient samples. *Nat Biomed Eng* (2022).
8. Ji, Y. *et al.* Multiplexed profiling of single-cell extracellular vesicles secretion. *Proc Natl Acad Sci U S A* **116**, 5979-5984 (2019).
9. Liu, C. *et al.* Low-cost thermophoretic profiling of extracellular-vesicle surface proteins for the early detection and classification of cancers. *Nat Biomed Eng* **3**, 183-193 (2019).
10. Zhang, P. *et al.* Ultrasensitive detection of circulating exosomes with a 3D-nanopatterned microfluidic chip. *Nat Biomed Eng* **3**, 438-451 (2019).
11. Shao, H. *et al.* New Technologies for Analysis of Extracellular Vesicles. *Chem Rev* **118**, 1917-1950 (2018).
12. Ning, B. *et al.* Liposome-mediated detection of SARS-CoV-2 RNA-positive extracellular vesicles in plasma. *Nat Nanotechnol* **16**, 1039-1044 (2021).
13. Liang, K. *et al.* Nanoplasmonic Quantification of Tumor-derived Extracellular Vesicles in Plasma Microsamples for Diagnosis and Treatment Monitoring. *Nat Biomed Eng* **1** (2017).
14. Zhu, L. *et al.* Coupling Aptamer-based Protein Tagging with Metabolic Glycan Labeling for In Situ Visualization and Biological Function Study of Exosomal Protein-Specific Glycosylation. *Angew Chem Int Ed Engl* **60**, 18111-18115 (2021).
15. Fan, X. *et al.* Cell-type-specific labeling and profiling of glycans in living mice. *Nat Chem Biol* **18**, 625-633 (2022).
16. Saxon, E. & Bertozzi, C.R. Cell surface engineering by a modified Staudinger reaction. *Science* **287**, 2007-2010 (2000).
17. Zhang, D. *et al.* Equipping Natural Killer Cells with Specific Targeting and Checkpoint Blocking Aptamers for Enhanced Adoptive Immunotherapy in Solid Tumors. *Angew Chem Int Ed Engl* **59**, 12022-12028 (2020).
18. Zheng, Y. *et al.* Enrichment-triggered prodrug activation demonstrated through mitochondria-targeted delivery of doxorubicin and carbon monoxide. *Nature Chemistry* (2018).
19. Stott, S.L. *et al.* Isolation of circulating tumor cells using a microvortex-generating herringbone-chip. *Proc Natl Acad Sci U S A* **107**, 18392-18397 (2010).
20. Reategui, E. *et al.* Engineered nanointerfaces for microfluidic isolation and molecular profiling of tumor-specific extracellular vesicles. *Nat Commun* **9**, 175 (2018).
21. Topalian, S.L., Taube, J.M., Anders, R.A. & Pardoll, D.M. Mechanism-driven biomarkers to guide immune checkpoint blockade in cancer therapy. *Nat Rev Cancer* **16**, 275-287 (2016).
22. Chen, L. & Han, X. Anti-PD-1/PD-L1 therapy of human cancer: past, present, and future. *J*

Clin Invest **125**, 3384-3391 (2015).
23. Yin, Z. *et al.* Mechanisms underlying low-clinical responses to PD-1/PD-L1 blocking antibodies in immunotherapy of cancer: a key role of exosomal PD-L1. *J Immunother Cancer* **9** (2021).
24. Poggio, M. *et al.* Suppression of Exosomal PD-L1 Induces Systemic Anti-tumor Immunity and Memory. *Cell* **177**, 414-427 e413 (2019).
25. Chen, G. *et al.* Exosomal PD-L1 contributes to immunosuppression and is associated with anti-PD-1 response. *Nature* **560**, 382-+ (2018).
26. Daassi, D., Mahoney, K.M. & Freeman, G.J. The importance of exosomal PDL1 in tumour immune evasion. *Nat Rev Immunol* **20**, 209-215 (2020).
27. Liu, Y. *et al.* Highly Sensitive Minimal Residual Disease Detection by Biomimetic Multivalent Aptamer Nanoclimber Functionalized Microfluidic Chip. *Small* **16**, e2000949 (2020).
28. Liu, Y. *et al.* Stimulus-Responsive Microfluidic Interface Enables Efficient Enrichment and Cytogenetic Profiling of Circulating Myeloma Cells. *ACS Appl Mater Interfaces* **13**, 14920-14927 (2021).
29. Grasselly, C. *et al.* The Antitumor Activity of Combinations of Cytotoxic Chemotherapy and Immune Checkpoint Inhibitors Is Model-Dependent. *Front Immunol* **9**, 2100 (2018).
30. Prescher, J.A., Dube, D.H. & Bertozzi, C.R. Chemical remodelling of cell surfaces in living animals. *Nature* **430**, 873-877 (2004).
31. Wang, H. *et al.* Selective in vivo metabolic cell-labeling-mediated cancer targeting. *Nat Chem Biol* **13**, 415-424 (2017).
32. Twyman-Saint Victor, C. *et al.* Radiation and dual checkpoint blockade activate non-redundant immune mechanisms in cancer. *Nature* **520**, 373-377 (2015).
33. Crescitelli, R., Lässer, C. & Lötvall, J. Isolation and characterization of extracellular vesicle subpopulations from tissues. *Nature Protocols* **16**, 1548-1580 (2021).

Acknowledgements

We thank the National Natural Science Foundation of China (Grants 22022409) and the Program for Changjiang Scholars and Innovative Research Team in University (Grant IRT13036) for their financial support.

Competing interests

The authors declare no competing interests.